

**Models of
postseismic
deformation**

O. Trubienko et al.

Models of postseismic deformation after megathrust earthquakes: the role of various rheological and geometrical parameters of the subduction zone

O. Trubienko¹, J.-D. Garaud², and L. Fleitout¹

¹Laboratoire de Géologie, ENS, 24 rue Lhomond, 75231 Paris Cedex 05, France

²Onera – The French Aerospace Lab, 92322 Châtillon, France

Received: 23 December 2013 – Accepted: 3 January 2014 – Published: 30 January 2014

Correspondence to: O. Trubienko (trubienko@geologie.ens.fr)

Published by Copernicus Publications on behalf of the European Geosciences Union.

Title Page

Abstract

Introduction

Conclusions

References

Tables

Figures

⏪

⏩

◀

▶

Back

Close

Full Screen / Esc

Printer-friendly Version

Interactive Discussion



Abstract

The postseismic deformations following subduction megathrust earthquakes are characterized by a horizontal velocity which, once non-dimensionalized by the coseismic displacement, increases with distance to the trench then presents an almost constant value for distances between 500 and 1500 km. The vertical velocity features a strong narrow peak on the trenchward side of the volcanic arc. Subsidence is observed in the far-field.

In order to understand better the implications of these observations, the influence of the geometry of low viscosity regions in subduction zones on the postseismic deformations is analyzed using a 2-D finite element model with viscoelastic rheologies. The slab dip in the top 80 km Θ_{top} , and deeper Θ_{bottom} and the locking depth all have a limited impact on the ratio of horizontal postseismic velocity over coseismic displacement. The smaller Θ_{bottom} , the smaller the amplitude of the predicted vertical velocity in the middle-field (200–500 km from the trench). The presence of the slab at asthenospheric depths affects very significantly both the horizontal and vertical velocities. Models with an 80 km thick lithosphere, where the relaxation occurs only in the asthenosphere, are characterized by a trenchward horizontal velocity decreasing very moderately in the middle-field and an uplift maximum on the continental side of the volcanic arc, at odds with the observations. A low viscosity channel (LVCh) over the deep parts of the subduction interface or a low viscosity wedge (LVW) have a considerable impact on the middle-field horizontal and vertical velocities: the trenchward horizontal velocities are very significantly increased while the vertical velocities are characterized by strong uplift over the deep parts of the subduction interface. In the case of a low viscosity wedge, a marked subsidence further away from the trench, on the continent side of the volcanic arc is predicted. While the low-viscosity wedge affects little the far-field horizontal velocities, the LVCh increases them significantly. The thicknesses of the lithosphere and the asthenosphere also have a strong impact on both the middle-field and the far-field velocities. The larger they are, the further from the trench are the maxima of the ratio

SED

6, 427–466, 2014

Models of postseismic deformation

O. Trubienko et al.

Title Page

Abstract

Introduction

Conclusions

References

Tables

Figures

◀

▶

◀

▶

Back

Close

Full Screen / Esc

Printer-friendly Version

Interactive Discussion



Models of postseismic deformation

O. Trubienko et al.

Title Page

Abstract

Introduction

Conclusions

References

Tables

Figures

⏪

⏩

◀

▶

Back

Close

Full Screen / Esc

Printer-friendly Version

Interactive Discussion



of the postseismic over coseismic horizontal displacement and of the far-field subsidence. 3-D modeling with a geometry as precise as possible of the various zones with postseismic creep associated with each megathrust earthquake is necessary to derive more precise conclusions. However, the 2-D modeling results obtained here, compared with postseismic data, point towards lithospheres and asthenospheres surprisingly similar in various areas of the world, with thicknesses around 70 and 200 km respectively and towards the presence of a LVW and/or a LVCh. The systematic description of the role of each parameter presented here will facilitate the choice of the parameters to vary in 3-D models.

1 Introduction

In recent years there have been several large subduction earthquakes (Sumatra 2004, Chile 2010, Japan 2011). Global Positioning System (GPS) provides for the first time precise measurements of deformations following these earthquakes and there is a large set of postseismic data available for those regions. What can we learn from these observations concerning the rheological structure of the mantle around subduction zones and about the process of stress accumulation and release associated with the seismic cycle? The concept of postseismic deformation linked to viscoelastic relaxation in the mantle has been put forward quite long ago (Thatcher and Rundle, 1984; Savage, 1983; Melosh and Raefsky, 1983). Most of these studies considered a fault with a 30° dip embedded in an elastic lithosphere overlying a viscoelastic half-space. The impact on the postseismic motion of the various geometrical and rheological factors characterizing an earthquake and its neighboring zone has not been studied thoroughly. It will be the object of the present paper.

A simple 2-D Cartesian model will be used. A complete 3-D model of each earthquake in spherical geometry should of course be performed in order to analyze the very rich datasets collected after the three recent giant earthquakes. However, the systematic analysis of the role of each geometrical and rheological parameter is more

Models of postseismic deformation

O. Trubienko et al.

Title Page

Abstract

Introduction

Conclusions

References

Tables

Figures

⏪

⏩

◀

▶

Back

Close

Full Screen / Esc

Printer-friendly Version

Interactive Discussion



readily obtained from simple 2-D models. The direction of horizontal velocities of stations located sideways cannot be studied with 2-D models. However, we have shown (Trubienko et al., 2013) that the main difference between 2-D and 3-D models for stations “in front” of the earthquake resides in the geometrical dispersion with distance inherent to 3-D vs. 2-D geometry. For example, once non-dimensionalized by the co-seismic value, horizontal velocities are similar in 3-D and 2-D.

The purpose of the present study is to get a first estimate of the parameters able to explain the general characteristics of the postseismic motions which will be described in Sect. 2. This general description of the role of each parameter will help interpreting results of 3-D models designed for each megathrust earthquake. From 2-D models, one can also learn what type of errors may (or may not) arise from uncertainties on the geometry of the problem, for example on the exact shape of the subduction interface. In the present paper, all models feature a low viscosity asthenosphere as the far-field postseismic motions observed away from the three recent giant earthquakes obviously require such asthenospheric relaxation. No postseismic slip is imposed on the subduction interface at seismogenic depths: such slip may be important to explain near-field motions, mainly during the first year after the earthquake, for example after Aceh earthquake (Fleitout et al., 2011) but it has not been included here as we are mainly interested in the postseismic motions a few years after the earthquake. Section 7 will consider a low viscosity channel which is somewhat similar to slip on the deep portions of the interface.

Some observational characteristics of postseismic deformations are described in Sect. 2. In Sect. 3 the finite element model set-up is briefly described. In Sect. 4, the effect of the slab dip at asthenospheric depths Θ_{bottom} on postseismic deformations is studied. Section 5 discusses the impact of Θ_{top} (the slab dip in the top 80 km) and Θ_{bottom} together. Section 6 describes how the locking depth affects surface deformations. In Sects. 7 and 8, the influences of low viscosity channels or wedges, and of lithospheric and asthenospheric thicknesses on the postseismic deformations are discussed.

2 Some characteristics of postseismic deformations

One of the important characteristics of the horizontal postseismic displacement is that it is roughly in the same direction as the coseismic displacement but its amplitude varies as a function of distance to the trench rather differently: for stations located in Japan and Asia at variable distances from the epicenter of Tohoku earthquake (Fig. 1), we have plotted the east component of the postseismic displacement non-dimensionalized by the local coseismic displacement (Fig. 2). The data over Japan come from time series provided by the GEONET GSI network. The data in Asia come from time series provided by the JPL website: <http://sideshow.jpl.nasa.gov/post/series.html>. We have subtracted a trend proportional to the preseismic velocities to keep only the effect of the earthquake (see Trubienko et al., 2013, appendix). All the data of displacement or velocity plotted on the various figures in this section are corrected for the preseismic velocity. We also plotted the displacement after 2.5 yr (still non-dimensionalized by the coseismic displacement) as a function of the distance of the station to the trench (Fig. 3). The postseismic over coseismic displacement ratio increases with the distance of the station to the trench until it reaches a plateau for distances larger than 500 km. This ratio seems to decrease for very large distances (larger than 1200 km) but the uncertainty on the postseismic velocity at very large distances is important.

On Fig. 5, examples of postseismic displacement divided by the coseismic displacement for stations in the far-field of Maule (LPGS and LHCL in Argentina), Tohoku (CHAN in China and SUWN in South Korea) and Aceh (PHUK and CHON in Thailand) are plotted: the data for LPGS, LHCL CHAN and SUWN are time series from the JPL website while the data for CHON and PHUK (located respectively close to Bangkok and at Phuket) come from campaign stations analyzed by Panumastrakul et al. (2012). (For Aceh and Maule, the location of the stations is shown on Fig. 4). The signal is very similar for all those GPS stations characterizing different earthquakes and located at distances between 500 km and 1600 km from the epicenter of the mega-earthquake which affects them. We found the same pattern for all the other stations in the far-field

SED

6, 427–466, 2014

Models of postseismic deformation

O. Trubienko et al.

Title Page

Abstract

Introduction

Conclusions

References

Tables

Figures

◀

▶

◀

▶

Back

Close

Full Screen / Esc

Printer-friendly Version

Interactive Discussion



in front of either Aceh, Maule or Tohoku that we could analyze: in spite of different dips of the subduction interface and potential differences in the asthenospheric viscosities and thicknesses, the far-field postseismic displacements are the same for the three mega earthquakes.

5 In the far-field, all these stations also subside after the megaequake. This has been studied in detail by Satirapod et al. (2013) using data in Thailand and Malaysia but is also visible in the far-field of Tohoku and Maule earthquakes although precise estimates of the subsidence rate are difficult to derive at present as these earthquakes are fairly recent and the vertical time series are rather noisy.

10 Horizontal and vertical velocities in NE Japan based on GEONET observations for the period 1 January 2012–30 December 2012 are plotted on Fig. 6. Japan is certainly the area where the “middle-field” postseismic motions monitoring is the densest. However, a similar pattern is observed in Chile and Sumatra area: it is characterized by horizontal postseismic velocities of large amplitude in the middle-field and vertical velocities presenting a peak on the trenchward side of the volcanic arc (see for example stations UMLH in Sumatra or ANTC in Chile on the JPL web site). In Chile, some stations on the coast (ARCO, CONT) exhibit subsidence.

15 In short, the pattern of postseismic velocities after a megaequake is similar for the three recent events. The horizontal displacement normalized by the coseismic displacement presents for the three earthquakes a pattern similar to that for Japan, presented on Fig. 5. The vertical velocity is characterized in the far-field by a marked subsidence, already rather large at a distance of 500 km from the trench (Satirapod et al., 2013). There is a narrow peak in vertical velocity on the seaward side of the volcanic arc. On the continentward side of the volcanic arc, the vertical velocities are moderate with a slight subsidence.

20 This similarity in the postseismic deformation pattern certainly points towards similar physical processes inducing postseismic motions. However the three regions do present different dips, in the top 70 km and at asthenospheric depths, and different mean depth of the coseismic slip. The differences in tomographic images between

Models of postseismic deformation

O. Trubienko et al.

Title Page

Abstract

Introduction

Conclusions

References

Tables

Figures



Back

Close

Full Screen / Esc

Printer-friendly Version

Interactive Discussion



for example South-America and the Sunda area may also suggest differences in asthenospheric viscosities (Debayle and Ricard, 2012). Numerical experiments exploring the role of the various rheological and geometrical parameters characterizing the subduction zones are necessary to understand better what this similarity in postseismic deformation pattern means.

3 Finite element model

In the present study we use our previously published 2-D finite element model of earthquake cycle in a viscoelastic Earth (Trubienko et al., 2013). It is characterized by the following features: an overriding plate and a subducting plate penetrating the mantle down to 470 km, an asthenosphere and a sub-asthenospheric mantle (Fig. 7). The modeled region is taken sufficiently large so that the solutions are not influenced by the mesh boundaries: the model is 8000 km broad and 1600 km deep.

The shear and bulk moduli increase with depth according to PREM in the whole model box. Both the overriding and subducting plate are elastic. The asthenosphere has a Maxwell viscosity $\eta = 3 \times 10^{18}$ Pas (we chose Maxwell for simplicity). The mantle below the asthenosphere is represented by a Maxwell viscoelastic layer with viscosities increasing exponentially from $\eta = 3 \times 10^{18}$ Pas at H_{mantle} to $\eta = 10^{21}$ Pas at 670 km. It is maintained at 10^{21} Pas in the lower mantle. From our previous studies (Fleitout et al., 2011; Satirapod et al., 2013), we think that a Burgers or generalized Burgers viscoelastic model is more appropriate. The time dependence of the displacement, and more specifically the curvature of this function, are indeed better described using a Burgers model, with a viscosity of the order $\eta = 3 \times 10^{18}$ Pas in the asthenosphere in the Kelvin-Voigt element governing the deformations on time-scales of the order of a few years. It can be seen in (Trubienko et al., 2013) that for the first few years, a Burgers model with a given transient viscosity η_0 and a Maxwell model with a long-term viscosity η_0 yield the same displacements during the first years of the cycle as long as μ_2 , the relaxed modulus of the Burgers body is a few times smaller than the elastic modulus. A short

Models of postseismic deformation

O. Trubienko et al.

Title Page

Abstract

Introduction

Conclusions

References

Tables

Figures



Back

Close

Full Screen / Esc

Printer-friendly Version

Interactive Discussion



Models of postseismic deformation

O. Trubienko et al.

Title Page

Abstract

Introduction

Conclusions

References

Tables

Figures

◀

▶

◀

▶

Back

Close

Full Screen / Esc

Printer-friendly Version

Interactive Discussion



term Burger rheology with a modulus in the Kelvin-Voigt element larger than the seismicological modulus may also be introduced to fit the velocity during the first months after the earthquake. Since here, we are interested in the geometry of the zones that creep on a time scale of a few years rather than in the time-dependence of this creep, we may use a Maxwell viscosity for simplicity. Also, we will assume that the asthenosphere below the overriding and subducting plate has the same viscosity. The stations on the subducting plates which register deformations linked to the megathrust earthquakes are scarce and situated far away from the earthquake so that the signal is very noisy. However, the rough estimates which can be obtained (see Fig. 5) suggest similar velocities on the oceanic and continental side. Also, when comparing results predicted by various models, we will not be interested in the relative amplitude of the velocities but again in their shape as a function of distance. One can easily rescale the curves by multiplying the viscosities by an appropriate factor: all figures presented below would stay perfectly unchanged if one divides the timescale and the viscosities by a same factor.

To produce an earthquake, in all the model cases presented here, we apply a uniform coseismic slip of 10 m from 0 down to D_{lock} on the subduction interface.

We determine five parameters that are related to the shape of the subducting slab and that can influence deformation during the seismic cycle. These are: H_{litho} (the thickness of subducting elastic plate), H_{asthe} (the thickness of asthenosphere), D_{lock} (the locking depth), Θ_{top} (the angle of subduction) and Θ_{bottom} (the slope of the subducting plate at depth), see Fig. 7. The subduction interface has a curved shape but the angle of subduction is defined as $\tan \Theta_{\text{top}} = \frac{H_{\text{litho}}}{L}$.

For Sects. 4–6 we assume that the thicknesses of the subducting plate H and overriding plate H_{litho} remain constant through all the computations ($H = H_{\text{litho}} = 80$ km). The asthenosphere is located beneath these plates (between 80 and 200 km depth, $H_{\text{asthe}} = 120$ km). In Sects. 4–6, the mechanical properties attributed to all the constitutive elements of the model remain constant. $D_{\text{lock}} = -40$ km for all the computations

in Sect. 4 and 5. In Sect. 6 we study the influence of D_{lock} on the postseismic signal; in particular $D_{\text{lock}} = -25$ km, $D_{\text{lock}} = -40$ km and $D_{\text{lock}} = -60$ km are considered.

In Sect. 7, we consider the potential effect of a LVCh or of a LVW with a Maxwell viscosity. The locking depth is then fixed to 26 km.

5 For Sect. 8, we vary H_{litho} and H_{asthe} , whereas the shape of subducting plate remains constant. In Sect. 8, $D_{\text{lock}} = 40$ km and the viscosity of the mantle below the asthenosphere is constant $\eta = 10^{21}$ Pa.s.

4 Effect of the dip of the subducting plate at asthenospheric depths on postseismic deformations

10 In this section we study the influence of Θ_{bottom} on the postseismic deformations.

We consider 3 values of Θ_{bottom} : model 1 with $\Theta_{\text{bottom}} = 35^\circ$, model 2 with $\Theta_{\text{bottom}} = 62^\circ$, model 3 with $\Theta_{\text{bottom}} = 75^\circ$ (Fig. 8). Above -80 km all the models have the same curved geometry. Below -80 km down to -470 km (the end of the slab at depth) the slope of the slab is controlled by the angle Θ_{bottom} . We also consider the case without
15 a slab at depth for comparison to some existing models based on spectral methods that assume that there is no elastic slab penetrating the asthenosphere.

Figure 9 depicts the postseismic response non dimensionalized by the coseismic response as a function of time for the 4 proposed models at 300 km and at 700 km from the trench. As observed, the non-dimensionalized horizontal velocities increase
20 with the distance to the trench as least for moderate distances.

The most noticeable difference among the four models, both at 300 km (“middle-field”) and at 700 km (“far-field”) away from the trench, can be seen between the model that does not have an elastic slab at depth and all the other models. The influence of the elastic slab at depth on interseismic deformations is discussed in Trubienko et al.
25 (2013).

We now compare models 1, 2 and 3. Since the subduction interface and all mechanical properties are identical, the coseismic displacement (not plotted here) is the

Models of postseismic deformation

O. Trubienko et al.

Title Page

Abstract

Introduction

Conclusions

References

Tables

Figures

◀

▶

◀

▶

Back

Close

Full Screen / Esc

Printer-friendly Version

Interactive Discussion



same for these three models. It should be noted that there is no significant difference between these models in the middle and far-field horizontal velocities for the first few years after the earthquake.

Horizontal and vertical velocities 2yr after the earthquake are plotted on Fig. 10.

The model with no slab at depth differs significantly from models 1, 2 and 3 (with slab) in the close- and middle-field. The assumption that there is no lateral viscosity variations linked to the presence of an elastic slab at depth leads to underestimating the postseismic signal on the overriding plate and to overestimating it over the subducting plate by up to 50 % in the middle and far-field.

Note that Melosh and Raefsky (1983) have already described the asymmetry in the horizontal velocities induced by the subducted slab at depth. In Melosh and Fleitout (1982), this asymmetry was attributed to the reaction of the elastic slab plugged in a viscous mantle which stretches back after the coseismic compression. The position of the negative and positive peaks of vertical velocity is at the same distance from the trench for the three “slab” models. However, the maximum value of these peaks is different: the steeper the slab, the larger the tendency for uplift.

To conclude, in a more general way, the angle of the elastic slab at depth affects mainly the vertical motion in the close and middle-field domain. The absence of slab at asthenospheric depths strongly affects both the horizontal and the vertical velocities in the close and middle field up to 500 km away from the trench. Including this slab in the model is thus essential. Small errors on the dip of the slab at depth induces some, but moderate, error on the predicted postseismic motions.

5 Effect of the dip of the subduction interface (shallow and deeper depths)

In Sect. 4, the effect of changing Θ_{bottom} only has been studied. Now we want to study how the angle Θ_{top} affects postseismic deformations. In this case a change of Θ_{top} is associated with a change of the downdip part of the slab and we keep the same values of Θ_{bottom} as in the previous section. The first case corresponds to the angles

Models of postseismic deformation

O. Trubienko et al.

Title Page

Abstract

Introduction

Conclusions

References

Tables

Figures

⏪

⏩

◀

▶

Back

Close

Full Screen / Esc

Printer-friendly Version

Interactive Discussion



$\Theta_{\text{top}} = 13^\circ$, $\Theta_{\text{bottom}} = 35^\circ$, the second case to $\Theta_{\text{top}} = 20^\circ$, $\Theta_{\text{bottom}} = 62^\circ$ and the third case to $\Theta_{\text{top}} = 26^\circ$, $\Theta_{\text{bottom}} = 75^\circ$ (see Fig. 11).

Figure 12a presents the horizontal coseismic displacement for these 3 models. The smaller the dip angle, the further from the trench the coseismic deformation spreads.

This is due to the fact that although the locking depth remains constant for all the cases, the locked zone extends over a broader zone away from the trench for smaller dips.

Figure 12b depicts the horizontal displacement 4 yr after the earthquake divided by the horizontal coseismic displacement. The curves have a similar amplitude (15% difference) and shape but with the peak displaced away from the trench for flatter interfaces. This fact has an important application to observed present day postseismic deformations in the regions of Sumatra, Chile and Japan. The observed far-field horizontal motion (divided by the corresponding coseismic displacement) is characterized by a similar amplitude for the three megathrust earthquakes (Fig. 5). The dip of the subducting slab is different in these regions (L is equal to 210 km for the Andaman subduction, 280 km near Sumatra, 230 km for Maule and 280 km for Tohoku). According to Fig. 12, this difference in slab dip should not induce any large difference in the non-dimensionalized horizontal velocity. Still, the slightly larger values for the east components of the stations PHUK and CHON might be related to the strong dip of the Andaman subduction. Differences of the order of 15% between the north-south and east-west postseismic motions of the far-field stations after Aceh earthquake are expected. Such errors are also expected if the along-strike changes in dip present both along the Tohoku subduction and the Maule subduction are neglected.

Figure 13 (bottom) shows that the extrema, positive and negative in the vertical velocities keep the same position with respect to the point where viscous relaxation begins (corner of the asthenospheric wedge, at distance L from the trench, marked by the vertical lines on Fig. 13). In particular, the positive peak in vertical velocity is always at a distance larger than L , even further than the site where the top of the slab reaches a depth of 100 km which often coincides with the island arc. This peak is more than 200 km broad. Neither the site nor the width of this peak seem to fit the observations

SED

6, 427–466, 2014

Models of postseismic deformation

O. Trubienko et al.

Title Page

Abstract

Introduction

Conclusions

References

Tables

Figures

⏪

⏩

◀

▶

Back

Close

Full Screen / Esc

Printer-friendly Version

Interactive Discussion



of vertical motion in Japan (Fig. 6). The maximum of the trenchward horizontal velocity over the overriding plate is approximately situated above the corner of the asthenospheric wedge (i.e. the point where the depth of the subduction interface equals the thickness of the lithosphere). We will see in the next sections that this remains true when other parameters (locking depth, thickness of the lithosphere) are varied.

6 Locking depth

In this section we study the effect of the locking depth on the postseismic deformations. To do this, we use our model 2 ($\Theta_{\text{top}} = 20^\circ$, $\Theta_{\text{bottom}} = 62^\circ$ from Fig. 11) and consider three different locking depths -25 km, -40 km and -55 km (red, blue and black dashed vertical lines respectively on Fig. 14). Velocities 2 yr after the earthquake are plotted on Fig. 15.

Before non-dimensionalization by the coseismic displacement, the solutions obtained from the three models have a very different amplitude. The deformation rates are higher for larger locking depths on both the overriding and subducting plates. Vertical subsidence is predicted above the end of the locked zone for a locking depth of 25 km whereas no subsidence is expected for 40 km and 55 km locking depths. This dependence of the vertical velocity on the locking depth has already been discussed by Melosh (1983). The curves of horizontal displacement non-dimensionalized by the coseismic slip are rather similar (bottom of Fig. 14). Notice that the position of the peaks in vertical velocity depends upon the configuration of the low viscosity asthenospheric wedge (Fig. 13) but little upon the position of the coseismic slip (Fig. 15).

7 Low viscosity channel and low viscosity wedge

Low Viscosity Wedges and Channels are formed in the subduction zones due to the dehydration of the subducting plate (Kawakatsu and Watada, 2007) and the serpentinization of the forearc mantle (Wada et al., 2008). These structures are imaged by

SED

6, 427–466, 2014

Models of postseismic deformation

O. Trubienko et al.

Title Page

Abstract

Introduction

Conclusions

References

Tables

Figures

◀

▶

◀

▶

Back

Close

Full Screen / Esc

Printer-friendly Version

Interactive Discussion



Models of postseismic deformation

O. Trubienko et al.

Title Page

Abstract

Introduction

Conclusions

References

Tables

Figures

◀

▶

◀

▶

Back

Close

Full Screen / Esc

Printer-friendly Version

Interactive Discussion



seismic tomography studies (Hyndman and Peacock, 2003). On the other hand, very recent studies have imaged a zone of strong P wave attenuation below the island arc in NE Japan (Nakajima et al., 2013). In short, it seems rather likely that either a serpentine low viscosity channel, a more bulky serpentine wedge or a zone of low viscosity due to melt below the island arc, modify the viscosity at relatively shallow depths (less than 80 km) in the region of the bottom of the interface.

Would these structures influence the pattern of postseismic deformations? To answer this questions, three models are compared: here, the “standard case” corresponds to the case 1 of Fig. 11 but with a locking depth of 26 km. (1) A LVCh is added to the standard case: this LVCh starts at a depth of 28 km and extends to the bottom of the subducting interface, with an average thickness of 15 km (Fig. 16, top). (2) A LVW is added to the standard case: the LVW starts at the same depth as the LVCh, and reaches the bottom of the overriding plate (80 km depth) and its maximum width is 90 km (Fig. 16, bottom). (3) The results for the standard case without a LVW or LVCh (Fig. 11, case 1) are shown for comparison.

LVCh and LVW are modelled with a Maxwell viscosity $\eta = 10^{18}$ Pas and $\eta = 3 \times 10^{18}$ Pas respectively. The locking depth for all the computations is 26 km, in particular the LVCh and the LVW do not overlap the earthquake slip zone.

Figure 18 shows the horizontal displacement 4 yr after the earthquake normalized by the horizontal coseismic displacement for all three cases. The predicted horizontal and vertical postseismic velocities 2 yr after the earthquake are also compared (Fig. 17).

Compared to the standard case, large horizontal velocities are observed for LVW and LVCh in the middle-field. Moreover, while the far-field horizontal velocities are not much affected by a LVW, they are considerably increased in the case of relaxation in a LVCh. Note that the point where the trenchward horizontal velocities are maximum is slightly displaced trenchward when a LVW or a LVCh are present.

For vertical velocities, there is a remarkable difference in the close- and middle-field. The models with LVCh and LVW predict an uplift in the area where relaxation begins (beginning of LVW or LVCh). LVW and LVCh have a somewhat similar effect on the

velocities (the increase in the far-field velocities in case of a LVCh can be compensated by a decrease of the viscosity). However, the LVW induces a broad and marked zone of subsidence on the continent side of the uplift peak while a LVCh does not.

The uplift of the Pacific coast stations of Tohoku (Fig. 6) is not well predicted by models with only relaxation in the asthenosphere. This uplift may be the consequence of the relaxation in a LVCh or LVW. Because both LVW and LVCh induce rather similar surface deformations, a more realistic 3-D model is required to reconstruct the shape and the location of these structures.

8 Mechanical thickness of lithosphere and asthenosphere.

Lithosphere-asthenosphere boundary

In the context of models of the seismic cycle, the terms lithosphere and asthenosphere are linked to mechanical properties over a time-scale of a few years and for deviatoric stresses of the order of 10^5 Pa. The mechanical boundary between lithosphere and asthenosphere may thus coincide with the bottom of the thermal boundary layer and thicknesses of the order of 80 km seem appropriate for a standard continental lithosphere or a mature oceanic lithosphere. Considering larger or smaller values is however relevant. The thickness of the low viscosity layer at the base of the plates is even more uncertain.

The first series of computer experiments in this section concern the mechanical thickness of lithosphere. We consider three values: $H_{\text{litho}} = 50$ km, $H_{\text{litho}} = 80$ km and $H_{\text{litho}} = 120$ km. For these three cases $H_{\text{asthe}} = 120$ km. Figure 19 shows the horizontal and vertical velocity two years after the earthquake. For thicker plates, the peak in vertical velocity is located further away from the trench (Fig. 19b). For thin plates, the horizontal displacement, divided by the coseismic displacement is close to zero 1200 km away from the trench, at odds with observations. Notice however that the peak in predicted vertical velocity is then closer to the trench: this peak is an indica-

Models of postseismic deformation

O. Trubienko et al.

Title Page

Abstract

Introduction

Conclusions

References

Tables

Figures

◀

▶

◀

▶

Back

Close

Full Screen / Esc

Printer-friendly Version

Interactive Discussion



tion of the presence of viscous relaxation in the depth range 40–80 km close to the subduction interface, whatever the origin of this relaxation.

Figure 20 shows the horizontal displacement after 4 yr, normalized by the coseismic displacement after the earthquake for $H_{\text{litho}} = 50$ km, $H_{\text{litho}} = 80$ km and $H_{\text{litho}} = 120$ km.

Vertical lines indicate the limit of the asthenospheric wedge, at a distance L from the trench.

To study the impact of the thickness of the asthenosphere on surface deformations, we consider four values: $H_{\text{asthe}} = 60$ km, $H_{\text{asthe}} = 120$ km, $H_{\text{asthe}} = 250$ km and $H_{\text{asthe}} = 600$ km. For these four cases $H_{\text{litho}} = 80$ km. As shown in Fig. 21 (a), the thinner the viscoelastic layer, the smaller is the predicted horizontal postseismic velocity in the far-field. Thick viscoelastic layers cause large uplift in the far-field (600 km from the trench) in contradiction with observations: as shown by Satirapod et al. (2013), Phuket subsides at a rate of 2 cm yr^{-1} while it is only some 500 km away from the trench. When the viscoelastic layer is thin (60 km), the horizontal displacement, divided by the coseismic displacement decreases too fast as a function of distance to the trench.

Figure 22 shows the horizontal displacement normalized by the coseismic displacement 4 yr after the earthquake for $H_{\text{asthe}} = 60$ km, $H_{\text{asthe}} = 120$ km, $H_{\text{asthe}} = 250$ km and $H_{\text{asthe}} = 600$ km. For thick asthenospheres (600 km or more), there is no maximum to the curve figuring the ratio of postseismic over coseismic displacement, in disagreement with observations (Fig. 3). However, with the standard asthenospheric thickness of 120 km, the horizontal velocity at large distances may decrease somewhat too fast. On Fig. 22, the normalized horizontal displacement is also plotted for the subducting plate. It presents the same shape as on the overriding plate but with an amplitude about 30 % smaller. This smaller amplitude is not visible on the data for the MCIL and DGAR stations plotted on Fig. 5. This may indicate an asthenospheric viscosity slightly lower below oceanic plates. The signal to noise for these far-away station is however too low to derive precise conclusions.

For all figures, (10, 13, 15, 17, 19), the maximum in horizontal velocity over the overriding plate is above the point where the plate interface reaches the depth of the bottom

SED

6, 427–466, 2014

Models of postseismic deformation

O. Trubienko et al.

Title Page

Abstract

Introduction

Conclusions

References

Tables

Figures

◀

▶

◀

▶

Back

Close

Full Screen / Esc

Printer-friendly Version

Interactive Discussion



of the overriding plate. According to Fig. 6 (bottom), this would mean that the “standard” lithospheric thickness used here is somewhat too large for Japan. A plate thickness of 70 km should be more appropriate. Figure 5 illustrates the fact that for the three major earthquakes, at distances ranging from 500 to 1000 km, the horizontal velocities non-dimensionalized by the coseismic velocity are very similar. This would not be compatible with large differences in the viscosity or the thickness of the asthenosphere or in the thickness of the lithosphere. Quite surprisingly, the mantles below Sundaland, Japan sea or South America appear to be rheologically similar.

9 Conclusions

This detailed analysis of the influence of the geometrical and rheological structure around subduction slabs on postseismic deformations (1) brought some constraints on the geometrical parameters important to take into account for a realistic modeling, and (2) gave a first idea of the geometrical characteristics of models able to fit the observed deformation.

We have shown that assuming no lateral viscosity variations linked to the presence of a subducting slab at depth strongly affects the postseismic signal. It is thus very important to include this subducting slab at depth in numerical models. The shape of the subduction interface and the locking depth do not affect very significantly the horizontal postseismic velocities non-dimensionalized by the coseismic displacement, except for a shift corresponding to the shift in the origin of the asthenospheric wedge for variable dip angles. The pattern of vertical velocity is more sensitive to those geometrical characteristics. A small error in the dip angle or in the average depth of the coseismic slip may not affect considerably the predictions of the horizontal velocities but it may alter the predictions of close and middle-field vertical velocities.

On one hand, the peak in vertical velocity predicted by models without LVCh or LVW poorly fits the observations because it is too broad and too far from the trench, except for cases with a thin lithosphere. On the other hand, cases with a thin lithosphere and

SED

6, 427–466, 2014

Models of postseismic deformation

O. Trubienko et al.

Title Page

Abstract

Introduction

Conclusions

References

Tables

Figures

◀

▶

◀

▶

Back

Close

Full Screen / Esc

Printer-friendly Version

Interactive Discussion



standard asthenosphere thickness fail in predicting sufficiently large far-field velocities. Models with a standard lithosphere but a thin (80 km) or thick (600 km) asthenosphere are also unable to reproduce the characteristics of the far-field deformation pattern. We have also tested cases with a thin lithosphere and thick asthenosphere but then the region of uplift around the peak in vertical velocity extends too far continentward.

Putting this together shows that models able to fit the postseismic data of megathrust earthquakes should feature either a LVW or a LVCh, or both. Thicknesses of the lithosphere and asthenosphere around 70 and 200 km respectively seem appropriate.

Acknowledgements. We thank GSI for providing us the GPS time series over Japan and E. Panumastrakul, W. Simons and C. Satirapod for the data in Thailand. This work has been supported by the ANR program “Flash-Japan” under contract ANR-11-JAPN-009, DYNTOHOKU.

References

- Debayle, E. and Ricard, Y.: A global shear velocity model of the upper mantle from fundamental and higher Rayleigh mode measurements, *J. Geophys. Res.-Sol. Ea.*, 117, doi:10.1029/2012JB009288, 2012. 433
- Fleitout, L., Garaud, J.-D., Cailletaud, G., Vigny, C., Simons, W., Ambrosius, B., Trisirisatayawong, I., Satirapod, C., and Song, G.: Postseismic deformations of the Aceh, Nias and Benkulu Earthquakes and the viscoelastic properties of the mantle, in: AGU Fall Meeting Abstracts, vol. 1, 2407 pp., 2011. 430, 433
- Hyndman, R. D. and Peacock, S. M.: Serpentinization of the forearc mantle, *Earth Planet. Sc. Lett.*, 212, 417–432, 2003. 439
- Kawakatsu, H. and Watada, S.: Seismic evidence for deep-water transportation in the mantle, *Science*, 316, 1468–1471, 2007. 438
- Melosh, H.: Vertical movements following a dip-slip earthquake, *Geophys. Res. Lett.*, 10, 47–50, 1983. 438
- Melosh, H. and Fleitout, L.: The earthquake cycle in subduction zones, *Geophys. Res. Lett.*, 9, 21–24, 1982. 436
- Melosh, H. and Raefsky, A.: Anelastic response of the Earth to a dip slip earthquake, *J. Geophys. Res.*, 88, 515–526, 1983. 429, 436

Models of postseismic deformation

O. Trubienko et al.

Title Page

Abstract

Introduction

Conclusions

References

Tables

Figures



Back

Close

Full Screen / Esc

Printer-friendly Version

Interactive Discussion



Models of postseismic deformation

O. Trubienko et al.

Title Page

Abstract

Introduction

Conclusions

References

Tables

Figures

⏪

⏩

◀

▶

Back

Close

Full Screen / Esc

Printer-friendly Version

Interactive Discussion



- Nakajima, J., Hada, S., Hayami, E., Uchida, N., Hasegawa, A., Yoshioka, S., Matsuzawa, T., and Umino, N.: Seismic attenuation beneath northeastern Japan: Constraints on mantle dynamics and arc magmatism, *J. Geophys. Res. Solid Earth*, 118, 5838–5855, doi:10.1002/2013JB010388, 2013. 439
- 5 Panumastrakul, E., Simons, W., and Satirapod, C.: Modelling post-seismic displacements in Thai geodetic network due to the Sumatra-Andaman and Nias earthquakes using GPS observations, *Surv. Rev.*, 44, 72–77, 2012. 431
- Satirapod, C., Trisirisatayawong, I., Fleitout, L., Garaud, J.-D., and Simons, W.: Vertical motions in Thailand after the 2004 Sumatra–Andaman Earthquake from GPS observations and its geophysical modelling, *Adv. Space Res.*, 51, 1565–1571, 2013. 432, 433, 441
- 10 Savage, J.: A dislocation model of strain accumulation and release at a subduction zone, *J. Geophys. Res.-Sol. Ea.*, 88, 4984–4996, 1983. 429
- Thatcher, W. and Rundle, J. B.: A viscoelastic coupling model for the cyclic deformation due to periodically repeated earthquakes at subduction zones, *J. Geophys. Res.*, 89, 7631–7640, 1984. 429
- 15 Trubienko, O., Fleitout, L., Garaud, J.-D., and Vigny, C.: Interpretation of interseismic deformations and the seismic cycle associated with large subduction earthquakes, *Tectonophysics*, 589, 126–141, 2013. 430, 431, 433, 435
- Wada, I., Wang, K., He, J., and Hyndman, R. D.: Weakening of the subduction interface and its effects on surface heat flow, slab dehydration, and mantle wedge serpentinization, *J. Geophys. Res.*, 113, B04402, doi:10.1029/2007JB005190, 2008. 438
- 20

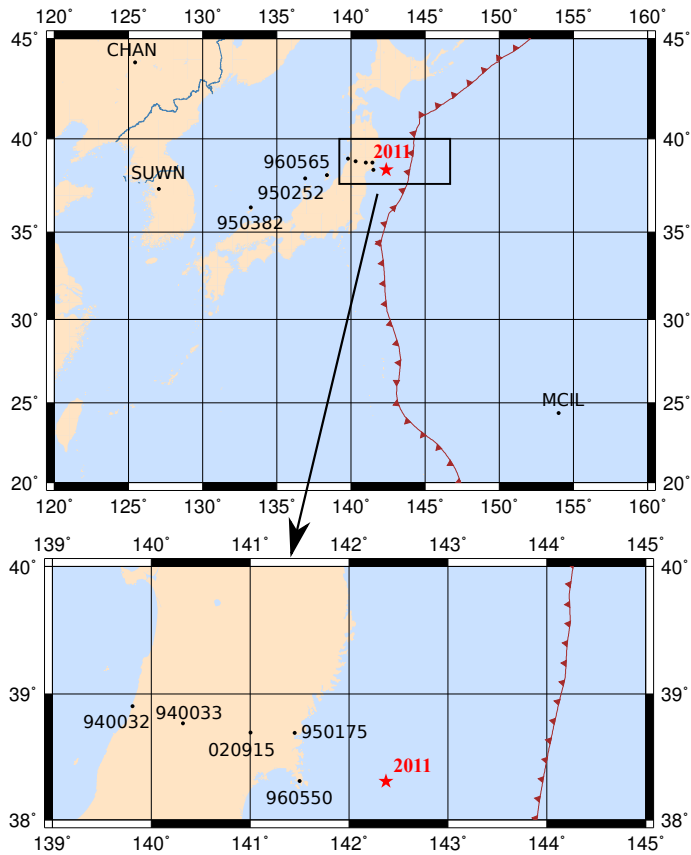


Fig. 1. Maps showing the location of the various stations for which the postseismic displacement is plotted on Fig. 2. These stations are at various distances from the trench. The red star indicates the epicenter of Tohoku earthquake. The bottom figure is a blow-up map showing the location of the stations closest to Tohoku epicenter.

Models of postseismic deformation

O. Trubienko et al.

Title Page

Abstract Introduction

Conclusions References

Tables Figures

◀ ▶

◀ ▶

Back Close

Full Screen / Esc

Printer-friendly Version

Interactive Discussion



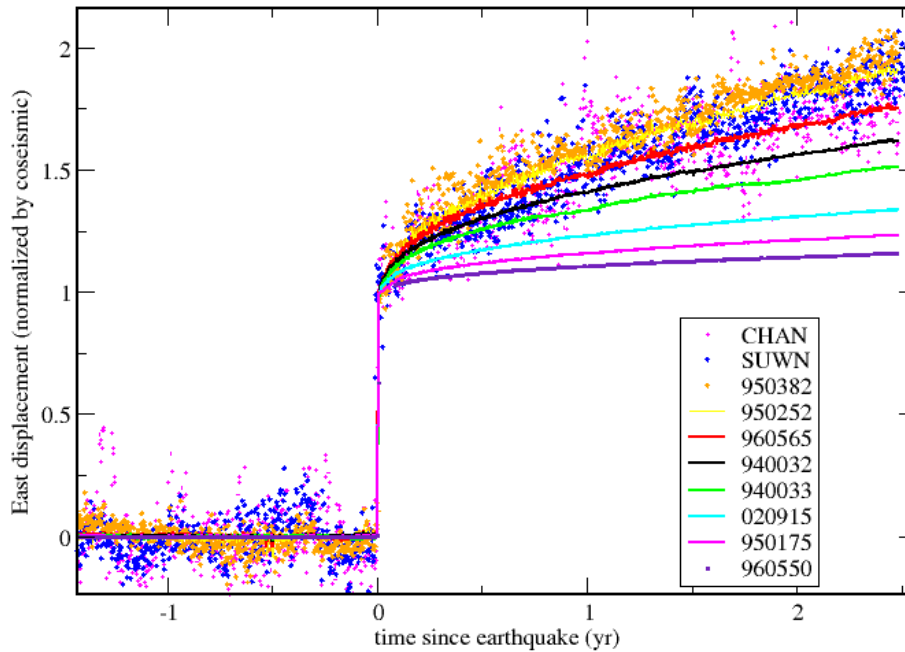


Fig. 2. Observed East displacement, as a function of time since Tohoku earthquake normalized by coseismic displacement for the stations plotted on Fig. 1.

Models of postseismic deformation

O. Trubienko et al.

Title Page

Abstract

Introduction

Conclusions

References

Tables

Figures

⏪

⏩

◀

▶

Back

Close

Full Screen / Esc

Printer-friendly Version

Interactive Discussion



**Models of
postseismic
deformation**

O. Trubienko et al.

Title Page

Abstract

Introduction

Conclusions

References

Tables

Figures

◀

▶

◀

▶

Back

Close

Full Screen / Esc

Printer-friendly Version

Interactive Discussion

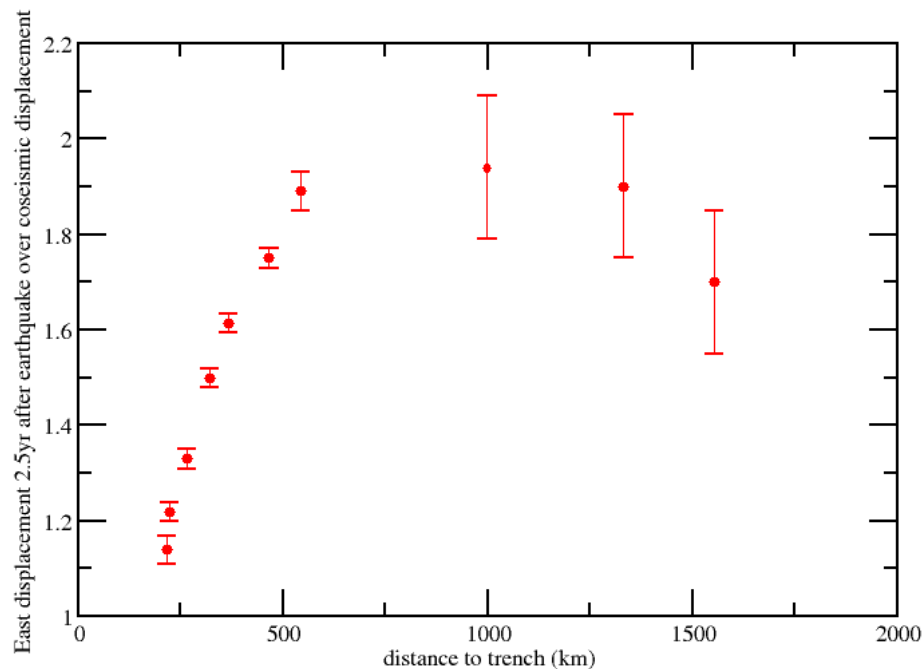


Fig. 3. Observed East displacement after 2.5 yr normalized by coseismic displacement for the stations of Fig. 1 as a function of distance to the trench.

Models of postseismic deformation

O. Trubienko et al.

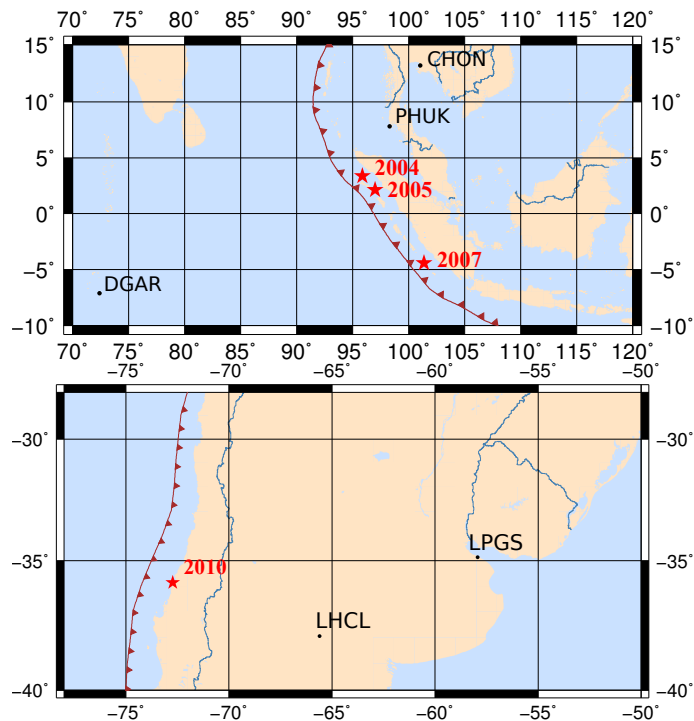


Fig. 4. Top: map showing the location of the stations CHON and PHUK for which the postseismic displacement is plotted on Fig. 5. The red stars indicate the epicenters of the 2004 Sumatra-Andaman, the 2005 Nias and the 2007 Bengkulu earthquakes. Bottom: map showing the location of the stations LHCL and LPGS for which the postseismic displacement is plotted on Fig. 5. The red star indicates the epicenter of the 2010 Maule earthquake.

Title Page

Abstract

Introduction

Conclusions

References

Tables

Figures

◀

▶

◀

▶

Back

Close

Full Screen / Esc

Printer-friendly Version

Interactive Discussion



Models of postseismic deformation

O. Trubienko et al.

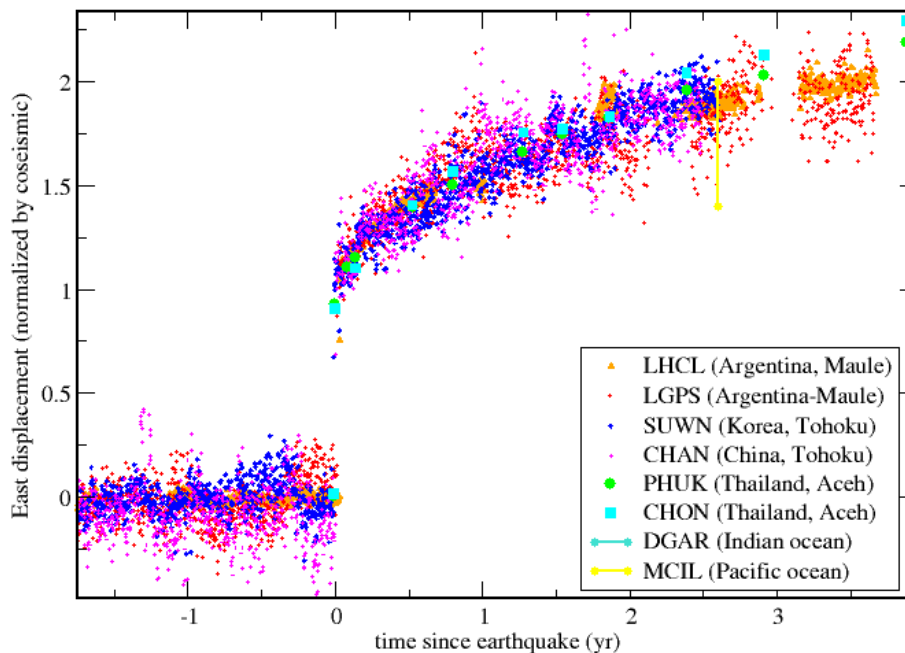


Fig. 5. Observed east displacement normalized by coseismic displacement for various stations on the overriding plate in the far-field of Maule (LHCL, LPGA), Tohoku (SUWN, CHAN) and Aceh (PHUK, CHON) as a function of time since the corresponding earthquake. An estimate of the normalized coseismic displacement is also provided for two far-field stations situated on the subducting plate (MCIL, Pacific ocean, North component and DGAR, Indian ocean, East component).

Title Page

Abstract

Introduction

Conclusions

References

Tables

Figures

◀

▶

◀

▶

Back

Close

Full Screen / Esc

Printer-friendly Version

Interactive Discussion



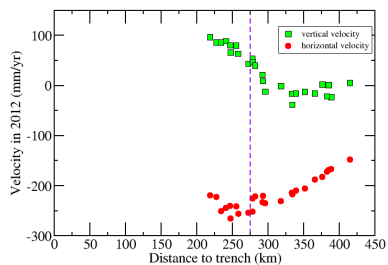
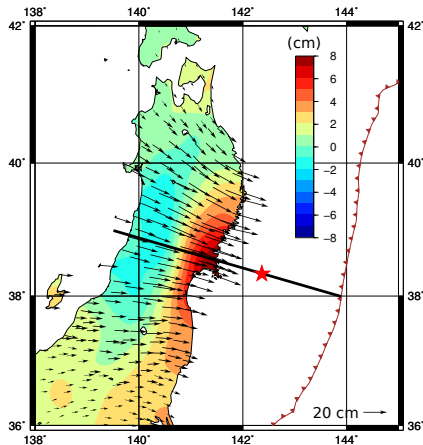


Fig. 6. Top: postseismic displacements registered by GEONET during the period 1 January 2012–30 December 2012. The black arrows show the horizontal postseismic displacements of the GPS sites. The color map shows vertical displacements. Bottom: horizontal and vertical velocities for stations located at less than 0.3° from the profile indicated by the black line on the top figure. The sign of the horizontal velocities has been chosen so that it corresponds to the sign on the model results of the next sections. The vertical dashed line indicates where the subduction interface reaches 80 km depth.

Models of postseismic deformation

O. Trubienko et al.

Title Page

Abstract

Introduction

Conclusions

References

Tables

Figures

◀

▶

◀

▶

Back

Close

Full Screen / Esc

Printer-friendly Version

Interactive Discussion



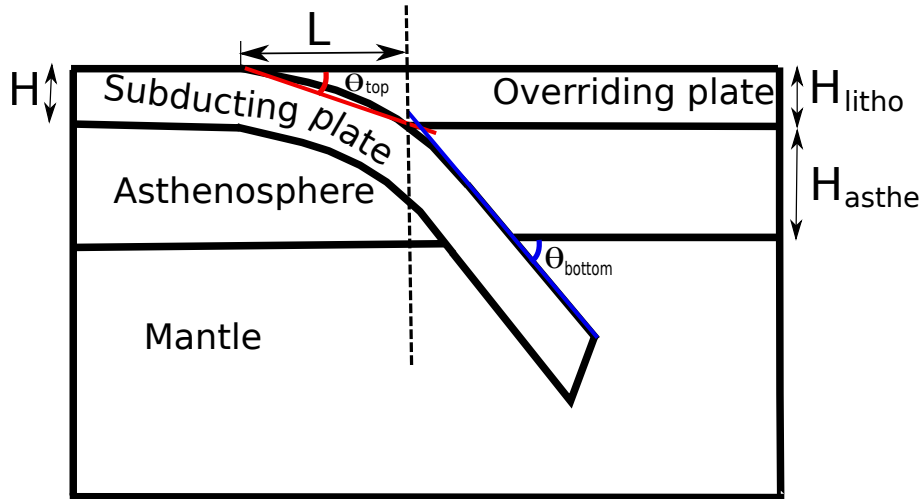


Fig. 7. Structural model close to the trench: subducting and overriding elastic plates, viscoelastic asthenosphere and mantle. Angle of subduction Θ_{top} and slope of the subducting plate at depth Θ_{bottom} .

Models of postseismic deformation

O. Trubienko et al.

Title Page

Abstract

Introduction

Conclusions

References

Tables

Figures

◀

▶

◀

▶

Back

Close

Full Screen / Esc

Printer-friendly Version

Interactive Discussion



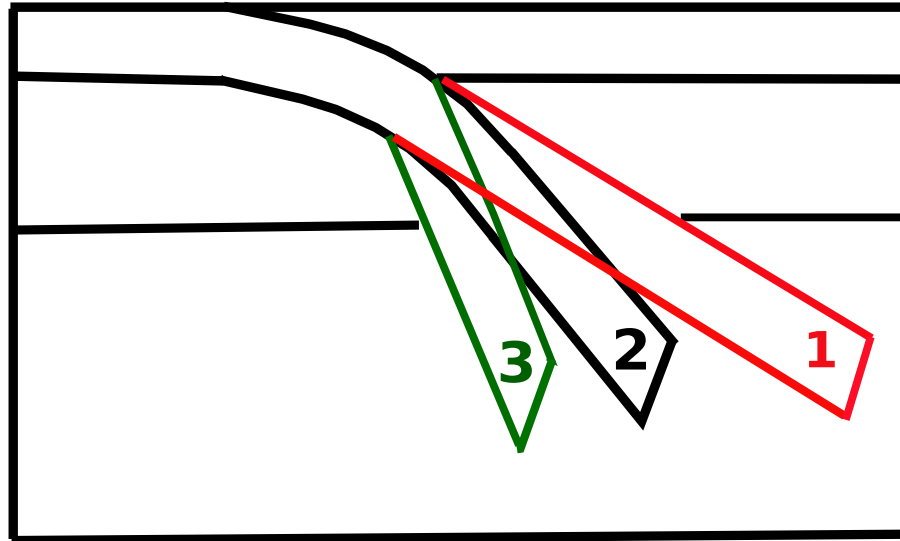


Fig. 8. Three structures of subducting slab: slab 1 with $\Theta_{\text{bottom}} = 35^\circ$, slab 2 with $\Theta_{\text{bottom}} = 62^\circ$, slab 3 with $\Theta_{\text{bottom}} = 75^\circ$.

Models of postseismic deformation

O. Trubienko et al.

Title Page	
Abstract	Introduction
Conclusions	References
Tables	Figures
◀	▶
◀	▶
Back	Close
Full Screen / Esc	
Printer-friendly Version	
Interactive Discussion	



Models of postseismic deformation

O. Trubienko et al.

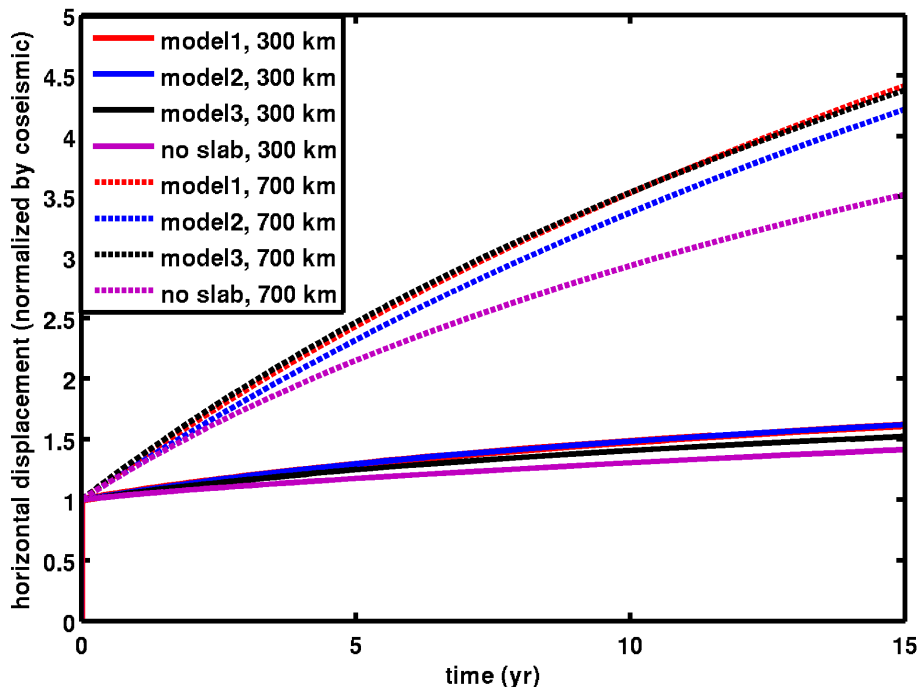


Fig. 9. Horizontal displacement non-dimensionalized by the coseismic displacement 0–15 yr after the earthquake for model 1 with $\Theta_{\text{bottom}} = 35^\circ$, model 2 with $\Theta_{\text{bottom}} = 62^\circ$, model 3 with $\Theta_{\text{bottom}} = 75^\circ$ and a case with no subducting slab at depth, at 300 km from the trench (full lines) and at 700 km from the trench (dashed lines) on the overriding plate. The coseismic displacements are 1.34 m at 300 km and 0.23 m at 700 km from the trench.

Title Page

Abstract

Introduction

Conclusions

References

Tables

Figures

◀

▶

◀

▶

Back

Close

Full Screen / Esc

Printer-friendly Version

Interactive Discussion



Models of postseismic deformation

O. Trubienko et al.

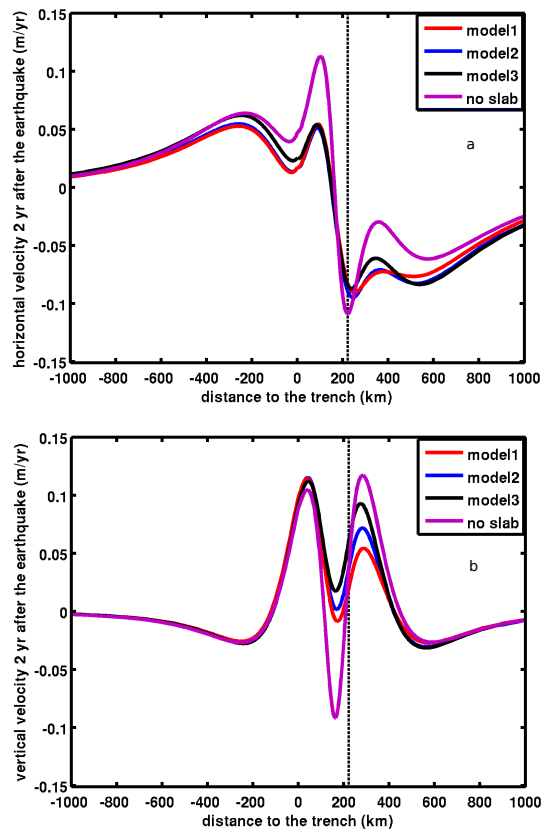


Fig. 10. Horizontal **(a)** and vertical **(b)** velocities 2 yr after the earthquake for model 1 with $\Theta_{\text{bottom}} = 35^\circ$, model 2 with $\Theta_{\text{bottom}} = 62^\circ$, model 3 with $\Theta_{\text{bottom}} = 75^\circ$ and a case with no subducting slab at depth. Vertical dashed line indicates the distance L (see Fig. 7).

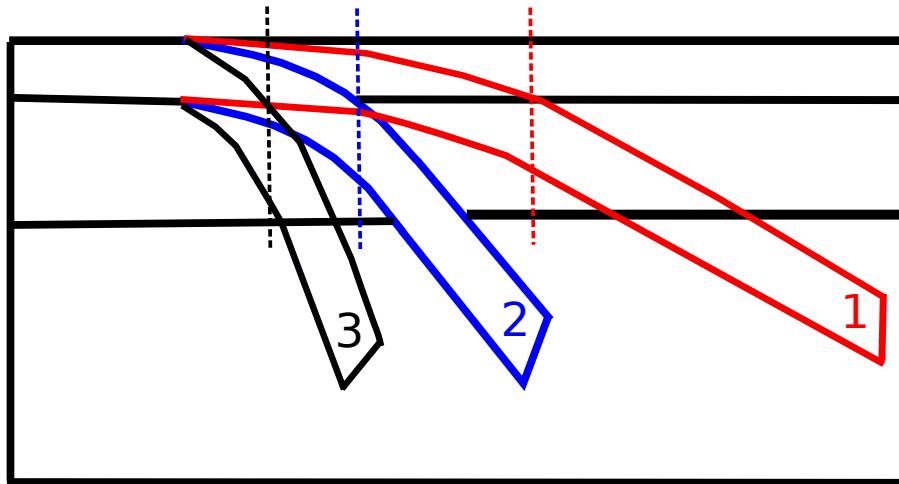


Fig. 11. Models: case 1: $\Theta_{\text{top}} = 13^\circ$, $\Theta_{\text{bottom}} = 35^\circ$, case 2: $\Theta_{\text{top}} = 20^\circ$, $\Theta_{\text{bottom}} = 62^\circ$, case 3: $\Theta_{\text{top}} = 26^\circ$, $\Theta_{\text{bottom}} = 75^\circ$. The vertical lines are located at a distance L from the trench for each case.

**Models of
postseismic
deformation**

O. Trubienko et al.

Title Page	
Abstract	Introduction
Conclusions	References
Tables	Figures
◀	▶
◀	▶
Back	Close
Full Screen / Esc	
Printer-friendly Version	
Interactive Discussion	



Models of postseismic deformation

O. Trubienko et al.

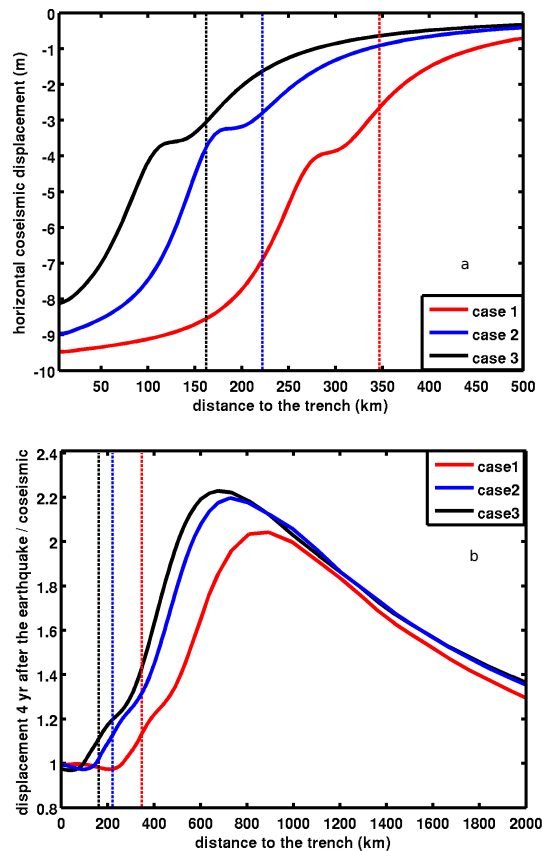


Fig. 12. Horizontal coseismic displacement **(a)** and horizontal displacement 4 yr after the earthquake divided by horizontal coseismic displacement **(b)** for case 1: $\Theta_{\text{top}} = 13^\circ$, $\Theta_{\text{bottom}} = 35^\circ$, case 2: $\Theta_{\text{top}} = 20^\circ$, $\Theta_{\text{bottom}} = 62^\circ$, case 3: $\Theta_{\text{top}} = 26^\circ$, $\Theta_{\text{bottom}} = 75^\circ$. Vertical dashed lines indicate the distance L from the trench for each case (Fig. 11).

Models of postseismic deformation

O. Trubienko et al.

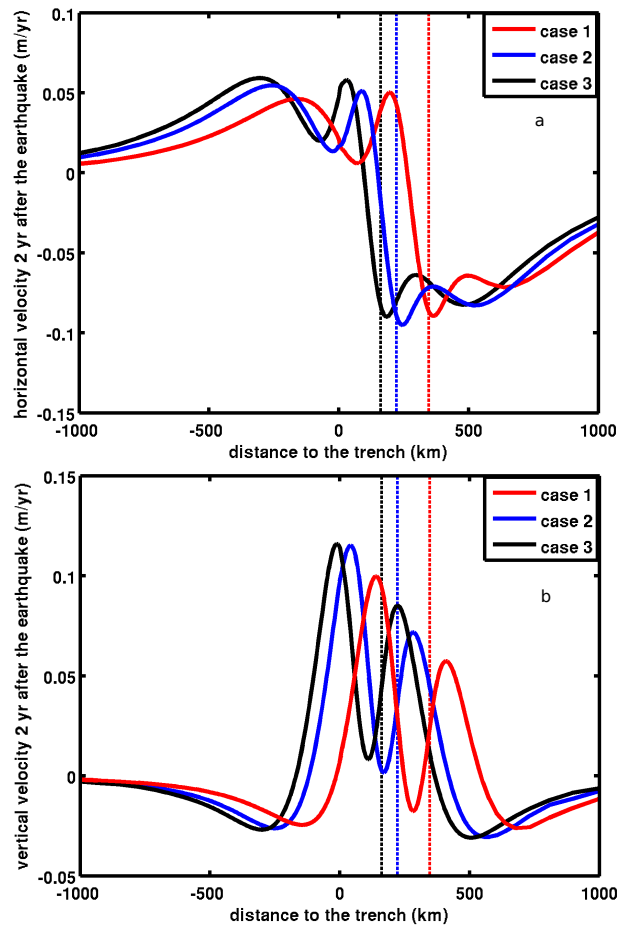


Fig. 13. Horizontal and vertical velocity 2 yr after the earthquake for case 1: $\Theta_{\text{top}} = 13^\circ$, $\Theta_{\text{bottom}} = 35^\circ$, case 2: $\Theta_{\text{top}} = 20^\circ$, $\Theta_{\text{bottom}} = 62^\circ$, case 3: $\Theta_{\text{top}} = 26^\circ$, $\Theta_{\text{bottom}} = 75^\circ$. Vertical dashed lines indicate the distance L from the trench for each case (Fig. 11).

Models of
postseismic
deformation

O. Trubienko et al.

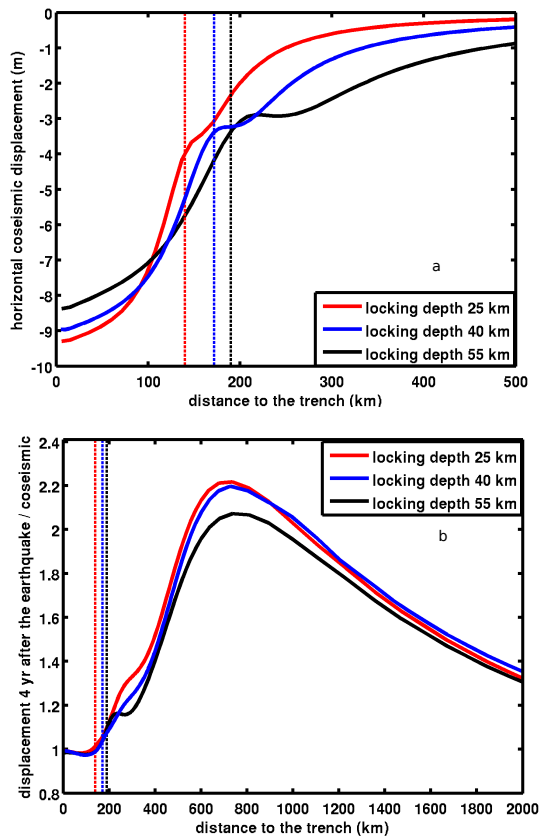


Fig. 14. Horizontal coseismic displacement **(a)** and horizontal displacement 4 yr after the earthquake divided by horizontal coseismic displacement **(b)** for locking depths of 25 km, 40 km and 55 km. Vertical lines shows the positions of the end of locked zones.

Models of
postseismic
deformation

O. Trubienko et al.

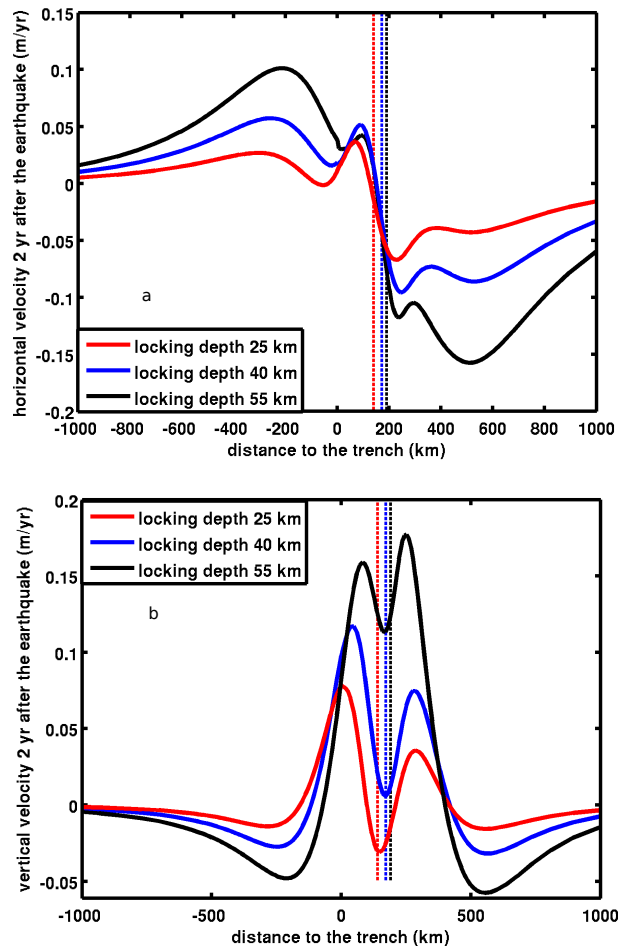


Fig. 15. Horizontal (a) and vertical (b) velocity 2 yr after the earthquake for locking depths of 25 km, 40 km and 55 km. Vertical lines are positions of end of locked zones.

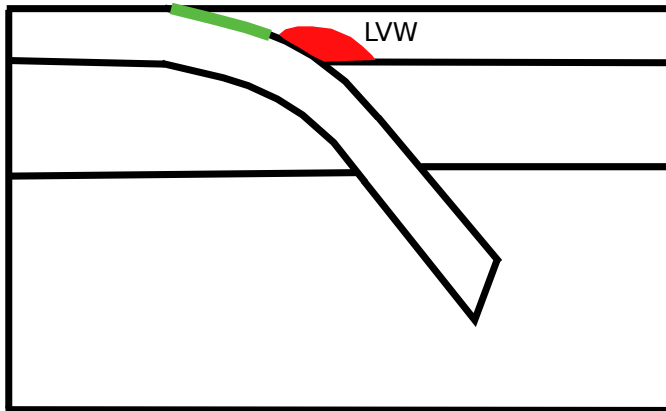
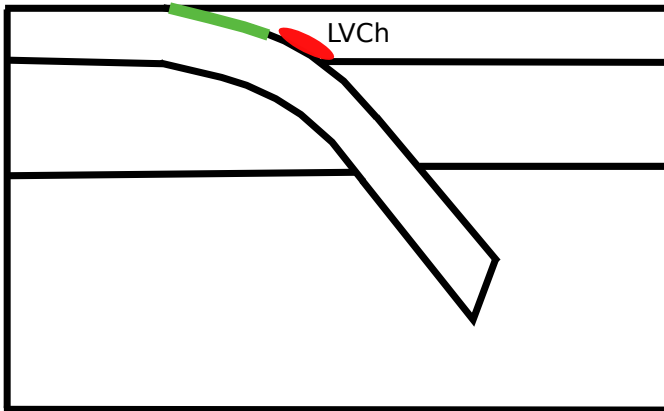


Fig. 16. Model structure for the cases with LVCh (top) and LVW (bottom). The green line indicates the fault zone.

Models of postseismic deformation

O. Trubienko et al.

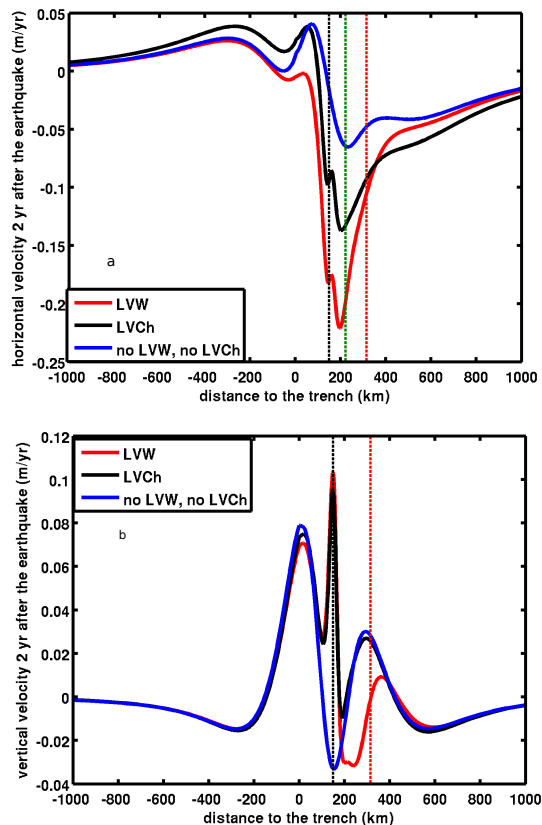


Fig. 17. Horizontal and vertical velocity 2 yr after the earthquake for the cases with LVW, LVCh and a case without LVW and LVCh. Vertical lines – beginning of LVCh (black), end of LVW (red), distance L from the trench (green).

Title Page

Abstract

Introduction

Conclusions

References

Tables

Figures

◀

▶

◀

▶

Back

Close

Full Screen / Esc

Printer-friendly Version

Interactive Discussion



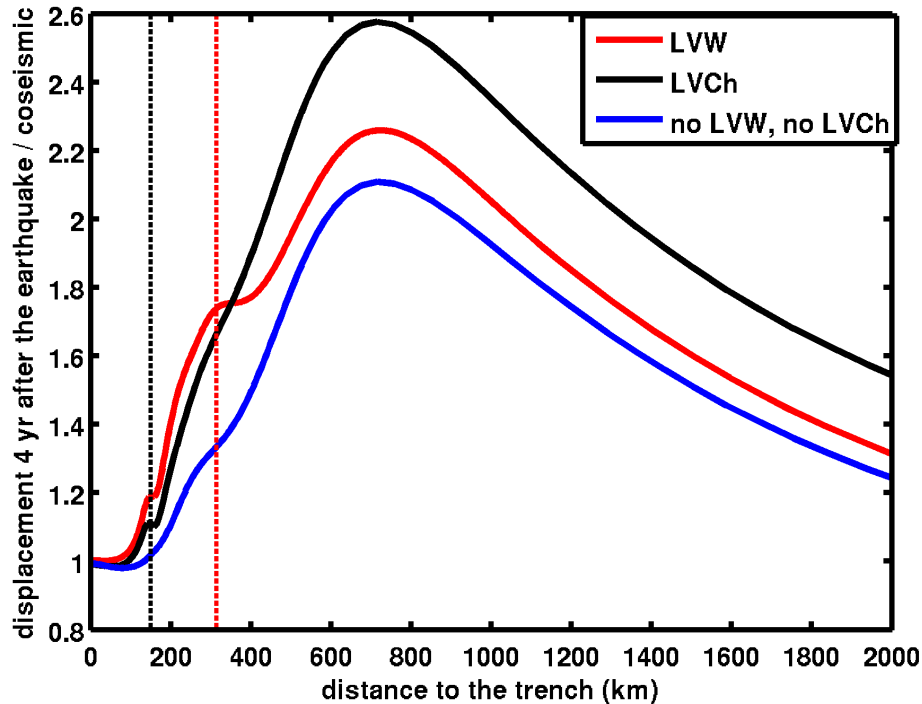


Fig. 18. Horizontal displacement 4 yr after the earthquake divided by horizontal coseismic displacement for the cases with LVW, LVCh and a case without LVW and LVCh. Vertical lines: beginning of LVCh and LVW (black), end (continentward) of LVW (red).

Models of postseismic deformation

O. Trubienko et al.

Title Page

Abstract Introduction

Conclusions References

Tables Figures

◀ ▶

◀ ▶

Back Close

Full Screen / Esc

Printer-friendly Version

Interactive Discussion



Models of postseismic deformation

O. Trubienko et al.

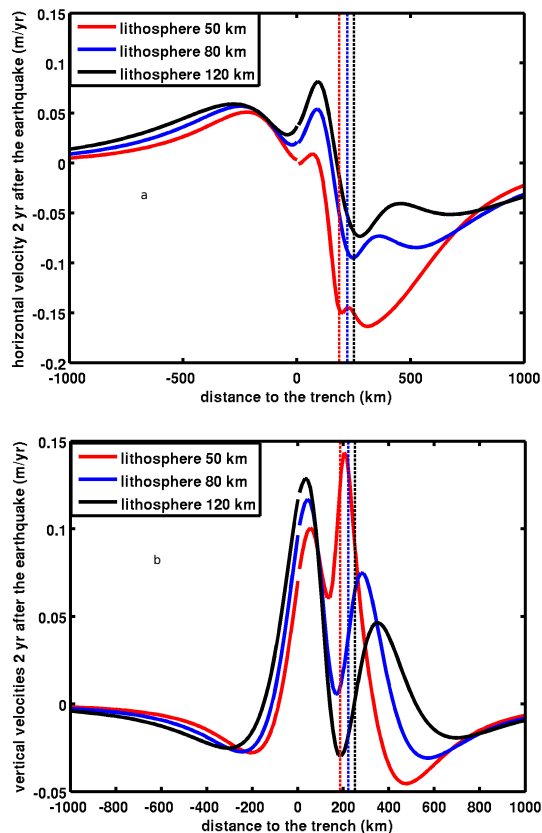


Fig. 19. Horizontal and vertical velocity 2 yr after the earthquake for $H_{\text{litho}} = 50$ km, $H_{\text{litho}} = 80$ km and $H_{\text{litho}} = 120$ km. Vertical lines indicate the distance L (beginning of the asthenospheric corner) for each case.

Title Page

Abstract

Introduction

Conclusions

References

Tables

Figures

◀

▶

◀

▶

Back

Close

Full Screen / Esc

Printer-friendly Version

Interactive Discussion



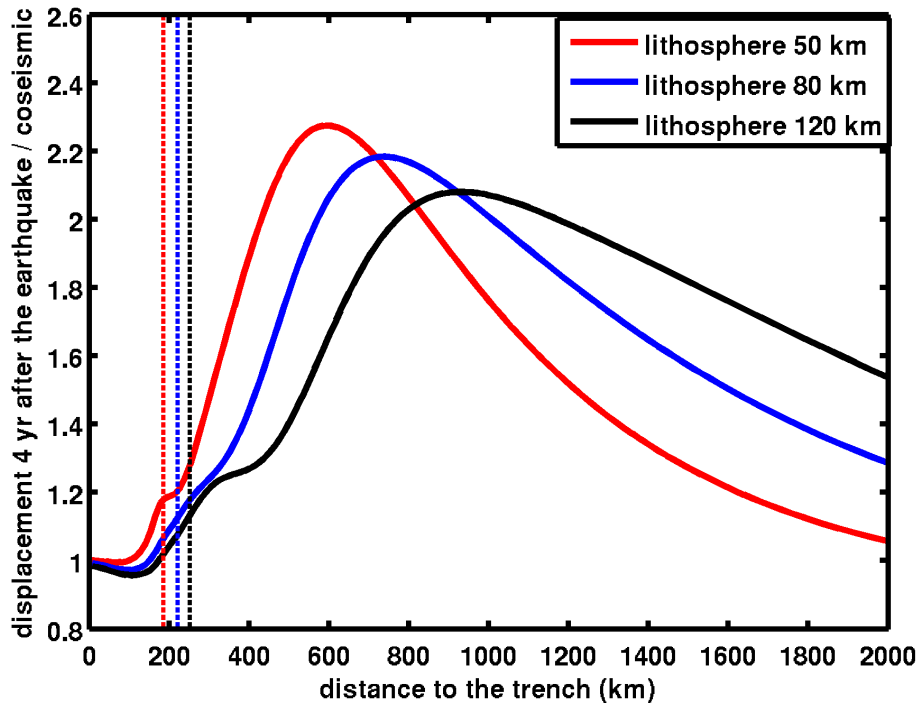


Fig. 20. Horizontal displacement divided by coseismic displacement 4 yr after the earthquake for $H_{\text{litho}} = 50$ km, $H_{\text{litho}} = 80$ km and $H_{\text{litho}} = 120$ km. Vertical lines indicate the limit of the asthenospheric wedge, at a distance L from the trench.

Models of postseismic deformation

O. Trubienko et al.

Title Page

Abstract Introduction

Conclusions References

Tables Figures

◀ ▶

◀ ▶

Back Close

Full Screen / Esc

Printer-friendly Version

Interactive Discussion



Models of postseismic deformation

O. Trubienko et al.

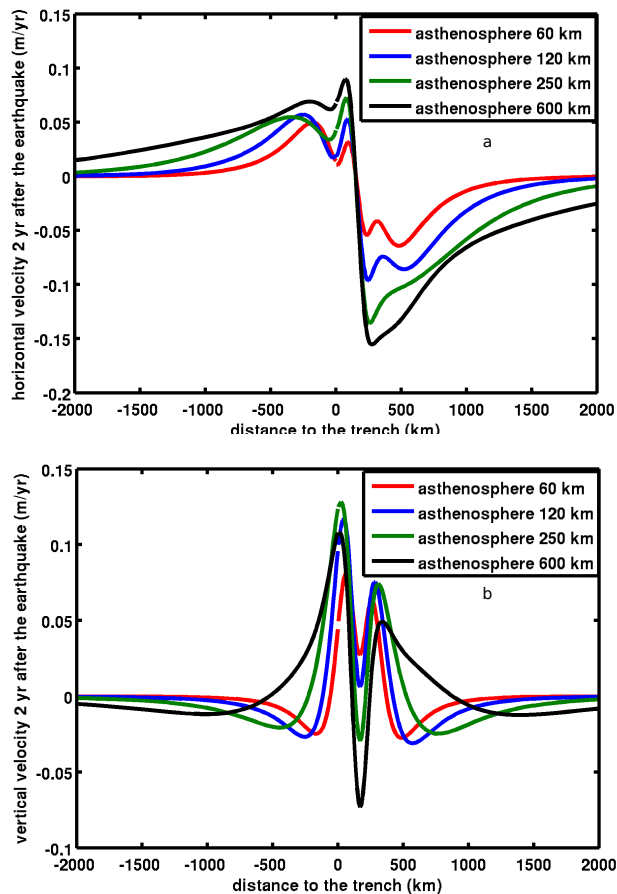


Fig. 21. Horizontal and vertical velocity two years after the earthquake $H_{\text{asthe}} = 60$ km, $H_{\text{asthe}} = 120$ km, $H_{\text{asthe}} = 250$ km and $H_{\text{asthe}} = 600$ km.

Title Page

Abstract

Introduction

Conclusions

References

Tables

Figures

◀

▶

◀

▶

Back

Close

Full Screen / Esc

Printer-friendly Version

Interactive Discussion



Models of
postseismic
deformation

O. Trubienko et al.

Title Page

Abstract

Introduction

Conclusions

References

Tables

Figures

◀

▶

◀

▶

Back

Close

Full Screen / Esc

Printer-friendly Version

Interactive Discussion

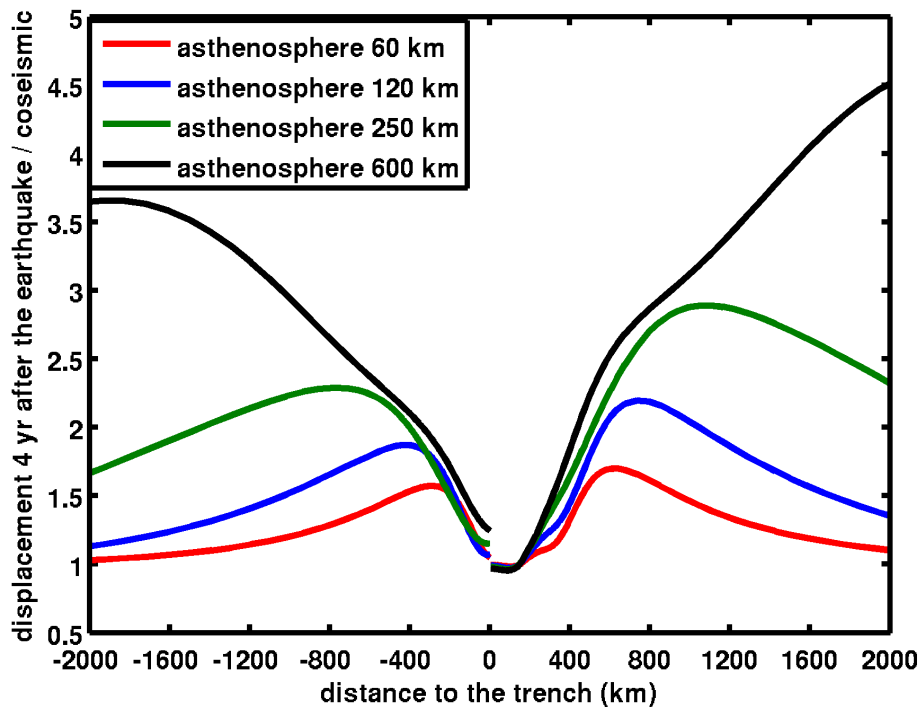


Fig. 22. Horizontal displacement normalized by coseismic displacement 4 yr after the earthquake for $H_{\text{asthe}} = 60$ km, $H_{\text{asthe}} = 120$ km, $H_{\text{asthe}} = 250$ km and $H_{\text{asthe}} = 600$ km.